LANGMUIR

pubs.acs.org/Langmuir

Article

Stability of Fluid Ultrathin Polymer Films in Contact with Solvent-Loaded Gels for Cultural Heritage

Amélie Castel, Philipp Gutfreund,* Bernard Cabane, and Yahya Rharbi*

Cite This: *Langmuir* 2020, 36, 12607−12619

Read Online

ACCESS | Metrics & More | Article Recommendations | Supporting Information

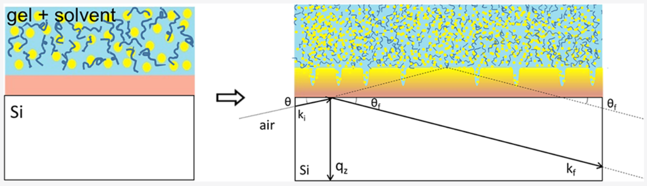

ABSTRACT: The removal of ultrathin amorphous polymer films in contact with an aqueous gelled solution containing small amounts of good solvent is addressed by means of specular and off-specular neutron reflectometry. The distribution of heavy water and benzyl alcohol is revealed inside Laropal A81, often employed as a protective varnish layer for Culture Heritage in the restoration of easel paintings. The swelling kinetics, interface roughness, and film morphologies were recorded as a function of temperature and increasing benzyl alcohol concentration in the dispersion of Pemulen TR-2, a hydrophobically modified acrylic acid copolymer. The addition of small amounts of good solvent results in the appearance of water-filled cavities inside the varnish, which grow with time. It is shown that while increasing the solvent concentration greatly enhances the hole growth kinetics, an increase in temperature above the glass transition temperature does not have such a big effect on the kinetics.

INTRODUCTION

Removing protecting thin glassy polymer films from a substrate is a critical step for numerous applications such as photonic band-gap materials,[1] microelectronics,[2] nanolithography,[3] and lab-on-chip devices.[4] It is also a particularly crucial step in the restoration of easel paintings and the one bearing the highest risk. Indeed, all surfaces of old paintings and many surfaces of the contemporary paintings are covered by polymer films (varnish), which act as a protecting barrier for the pictorial layer against environmental exposure. However, due to natural ageing, external and environmental factors (dirt, light, humidity), these layers undergo irreversible changes over time. Consequently, the esthetic and artistic aspects of the pieces of art change irreversibly due to (micro-)cracks, color changes, oxidation, etc.

Hence, regular restoration of the altered varnish layer is needed. A common restoration procedure consists of manually transferring a good solvent to soften the altered varnish layer and mechanically removing it by abrasion. During this process, the risk of irreversible damage of the pictorial layer underneath is very high because of the following two factors: (1) the solvent diffusion in thin layers is difficult to control and (2) collapsing the fragile granular structure of the pictorial layer under excessive stress during manual abrasion could also lead to nonvisual but irreversible structural damages affecting its stability.[5−10] Therefore, there is an urgent need to conduct precise investigations of the physical mechanisms involved during the various restoration steps.[8,11,12]

To limit the amount of aggressive solvent in the cleaning process, it was proposed to work in so-called "mild conditions" by diluting the solvent with water.[13] However, the results preceding this work on such binary mixtures obtained by neutron reflectometry (NR)[14] showed that above a solvent fraction of 0.3%, the water invades the whole film through a dewetting-type process, destroying the entire varnish and exposing the underlying layer to the bare liquid. On the other hand, at the beginning of the 1990s, to reduce the capillary penetration and the concentration of liquid solvents on surfaces, Wolbers suggested to increase the viscosity of the products using polymer solutions as a matrix for the cleaning agent, so-called Wolbers gels.[15] The high viscosity of the gel and the low concentration of the solvent allow reducing the action of the solvent significantly, such as its penetration power. Thanks to the increase in the retention time of the products/solvents maintained in the gel matrix, the product is slowly transferred and the restorer can adapt the gel/surface contact time. Quite quickly, these gels were commonly employed in cultural heritage conservation.[16] Gels have been widely studied because of their applications in numerous industries such as cosmetics, food, health, and even in products for safety (bulletproof vests). New innovating gels emerged, which could be suitable in art restoration like tough gels,[17] microemulsion gels,[18] emulsion gels,[19] and nanogels.[20] In two recent reviews, Baglioni et al. emphasized chemically cross-linked gels as a promising tool for the conservation of cultural heritage.[21,22] In contrast to the here studied Wolbers gels,

Received: July 22, 2020
Revised: September 29, 2020
Published: October 12, 2020

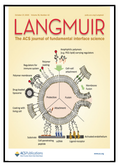

https://dx.doi.org/10.1021/acs.langmuir.0c02162
Langmuir 2020, 36, 12607−12619

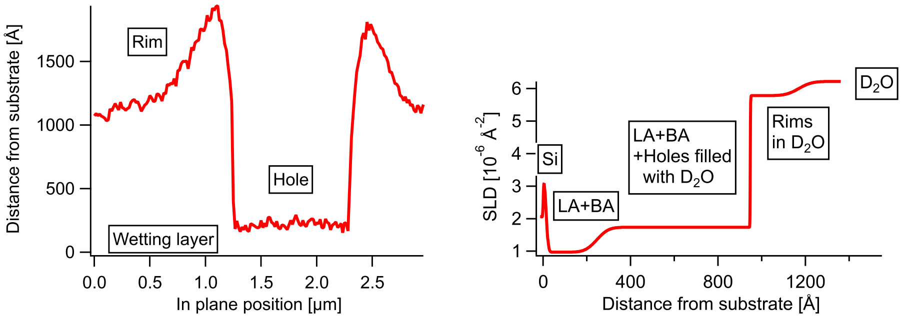

Figure 1. (Left) Surface height versus in-plane position across a dewetting hole as seen by atomic force microscopy (AFM) in air of a LA film after prolonged exposure to a water/BA binary mixture. (Right) Fitted scattering length density (SLD) of a similar LA film in a BA/water mixture versus distance from the substrate. Note that the annealing time is longer for the AFM measurement, leading to significantly larger holes and rims. This data is taken from ref 14.

chemical gels do not need subsequent cleaning after application to remove the gelling polymer residues from the surface. However, the application of gels in general and their effectiveness to remove nonoriginal materials on a macroscopic scale are impressively demonstrated by visual images, the potential microscopic penetration of liquids into the original layers, and therefore potentially irreversible changes are not investigated. In addition, after transferring a small amount of solvent by a gel into varnish, a mechanical action must follow to remove the swollen varnish. This step obviously bears risks on its own.

From a scientific viewpoint, film removal seems straightforward in thick films where diffusion times and distances are macroscopic. However, the solid-to-liquid transition of polymers may be quite different from nonpolymeric materials. Unlike nonpolymeric materials, polymers do not dissolve instantaneously and the classic dissolution process of a polymer involves transport processes, namely, solvent diffusion and disentanglement of the polymer chains.[23] The first stage is penetration of a few solvent molecules that plasticize the polymer. As a result, the macromolecules can cross the polymer/solvent interface. If the molecular weight of the polymer is high enough, they will form a gel layer at the surface of the film. The next stage is the disentanglement of the macromolecules and their escape from the gel layer into the solvent. But there are also cases where the polymer cracks before any gel layer is formed.[24]

In the case of ultrathin films, the situation is more complex as surface effects and reduced dimensionality may affect the physical properties of the polymer, such as chain conformation, glass transition temperature, and polymer dynamics.[25] Van der Waals interactions of the substrate may also play a role in these thin films.[26] And, last but not least, many films may become unstable below a certain threshold thickness, leading to dewetting when heated close or above their glass transition temperature (T_g).[27] The phenomenon of dewetting is relatively well studied for unpolar polymer films,[28] but systems with a significant amount of polar groups, as the case in the present study, may significantly alter the film stability.[29−31]

The use of a single solvent is the easiest case of polymer film dissolution. In this study, however, a binary solvent−nonsolvent mixture suspended in an emulsifier solution is used. The case of a binary solvent without the emulsifying copolymer was already studied before[14] and revealed a dewetting-type polymer film removal due to the different surface affinities of the solvents. Using viscosity-enhancing emulsifiers to promote thin film removal, as studied here, generates new challenges in polymer physics and raises particularly one important question about the emulsification mechanisms in confined media. Due to the presence of the copolymer, the matrix is now able to absorb the hydrophobic polymer layer in the form of an emulsion.[32,33] This increases the diversity of chemical interactions in the system and may shift the solvent partitioning.

Similar to our previous study,[14] we will determine the solvent penetration inside the polymer and follow the film break-up using specular and off-specular neutron reflectometry (NR).

NR was found to be an effective technique that gives both structural and chemical information, thanks to targeted hydrogen/deuterium (H/D) labeling. It is an ideal tool to observe the solvent penetration in real-time and has already proven this in similar experiments.[14,34−36] It is a nondestructive and noninvasive technique for the investigation of thin polymer films, liquid/solid and liquid/liquid interfaces with a resolution of a few Ångströms. In addition, NR can be linked to a complex sample environment like cone/plate rheology,[37] as was done here as well. In contrast to our previous study,[14] we cannot easily complement NR by microscopy as the gel cannot be removed from the film after application without destroying the system.

As in our previous study,[14] we will use ultrathin (∼100 nm) polymer films of Laropal A81 (LA), a resin commonly used as a varnish on paintings, in contact with a small quantity of benzyl alcohol (BA) dissolved in a bulk aqueous solution. In the preceding study, we observed swelling of the varnish layer by BA penetration at small BA quantities in the water matrix and dewetting of the varnish by the appearance of holes, as depicted in Figure 1, at a BA concentration above 0.3% BA at room temperature (RT). The dewetting process, however, showed the following two remarkable differences when compared to the dewetting of polymer films from solids in air: (a) the wetting layer underneath the holes was unusually thick (see Figure 1) and (b) clear loss of polymer at the late stages of dewetting was observed. We identified the affinity of the water matrix to the hydrophilic substrate underneath the hydrophobic polymer to be the driving force for the film instability when in contact with the BA/water binary solution. The fact that the dewetting process started only above a threshold BA concentration in water led us to speculate about the plasticizing effect of BA inside the polymer film by reducing its glass transition temperature close to room temperature and initiating polymer flow. In the present

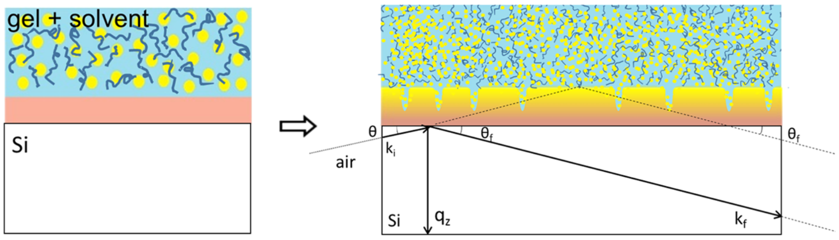

Figure 2. Sketch of the experiment. The yellow dots represent the solvent (BA) and the blue chains the Pemulen molecules. Note that the reflection angles are exaggerated for illustration. Also, the lengths of the incoming (k_i) and outgoing (k_f) wave vectors are identical in elastic scattering. On the right-hand side, water-filled holes with finite depth inside the varnish are illustrated.

study, we will vary the temperature significantly above T_g to test this hypothesis.

The second difference in the current study is the addition of a gelling agent to the aqueous phase, Pemulen TR-2, as proposed for varnish removal in art restoration. Unlike the earlier studied case of water/solvent mixtures, the case of physical gels containing the solvent is indeed used in Cultural Heritage; therefore, the latter system is closer to the real application.

Finally, to go toward the abrasion of the swollen varnish, we will test the influence of gentle mechanical stress on the system by shearing the sample in a rheometer and watching it with NR *in situ*.[37]

■ EXPERIMENTAL SECTION

Materials. Laropal A81 (LA) from BASF[38] is a synthetic polymer resin synthesized from urea, isobutyraldehyde, and formaldehyde and is a reference varnish in cultural heritage because of its stability, resistance, and transparency.[39] The LA structure was reported to consist of 4-hydroxy-6-isopropyl-5,5-dimethyl-tetrahydropyrimidin-2(1*H*)-one and aldehydic compounds.[40] LA is a small molecular weight polymer with a typical weight-average molecular weight (M_w) of 3640 Da and number-average molecular weight (M_n) of 1266 Da as deduced from gel chromatography (GC).[41] The T_g measured by differential scanning calorimetry (DSC) is 48 °C.[14] Benzyl alcohol (Sigma-Aldrich, 99.8%), deuterated water (D_2O, Eurisotop ref D214L, 99,9% D), Pemulen TR-2 (Lubrizol), and triethanolamine (TEA, 98%, CTS France[42]) were used as received. Pemulen TR-2 (PTR-2)[32,33,43,44] is an anionic polymeric emulsifier[33] made of a slightly cross-linked acrylic acid backbone ($-[CH_2-CH-(COOH)-]_n-$) and few hydrophobic pendant alkyl molecules, 10−30 carbons long. It is used as a primary emulsifier and a viscosity-enhancing agent.[45] Triethanolamine (TEA) from CTS, a ternary amine used in cosmetic and art restoration applications, is used as a buffering agent for Pemulen gel preparation.

Thin Film Preparation and Characterization. To make ultrathin polymer films, LA/toluene mixtures of 20 g/L were deposited by spin coating using a Delta 6 RC TT (SÜSS MicroTec Lithography GmbH)[46] at 2500 RPM for 44 s onto silicon crystal blocks (5 × 5 × 1 cm^3 (111) from Sil'Tronix France or 7 × 7 × 1 cm^3 (100) from Crystec, Germany) rigorously cleaned following a precise protocol (20 min in deionized water, acetone, ethanol, formaldehyde, and water). These films were subsequently annealed at 114 °C for 30 min in a vacuum oven. During this heating process, all of the toluene is evaporated and an apparent homogeneous film of LA is observed. The film thickness measured by ellipsometry is 74 ± 1 nm. These films did not show any apparent dewetting by optical microscopy. The films were subsequently placed in contact with different concentrations of BA (0, 0.3, 0.5, 0.6, and 0.7%) in D_2O with Pemulen TR-2 gel at pH 7 (adding TEA) and observed by NR as a function of shear, time, and temperature.

Preparation of the Gelly Matrix. The LA film was studied in contact with a polymer solution of Pemulen TR-2 from CTS France (Lubrizol). This dispersion is prepared by following the suggestions from Stravroudis[44] at 0.1% of PTR-2 in D_2O at pH 7. First, 0.1 wt % dry powder of PTR-2 is mixed with water and dispersed by stirring it overnight to obtain a uniform mixture. Then, the final pH of the preparation is adjusted by adding some drops (about 0.1% in total volume) of TEA previously dissolved in D_2O to the PTR-2/D_2O mixture until reaching a homogeneous solution of pH 7 ± 0.2.[32,44] Then, a chosen amount of BA is added to the polymer solution, mixed for 1 h, and left for 48 h at room temperature. At 0.1% PTR-2, the solution has a low viscosity and it can flow through the tubing connected to the reflectometry cells.

NR Experiments. Neutron reflectometry (NR) was performed to extract the vertical swelling of the polymer film by directing a collimated neutron beam at the Si/LA/W interfaces through the Si block and measure the reflected intensity as a function of momentum transfer normal to the interface. For a short introduction of NR on the here studied system, the reader is referred to our previous publication.[14]

NR experiments were performed on the time-of-flight (ToF) reflectometer FIGARO[47] at the Institut Laue-Langevin (ILL), Grenoble, France. The samples were either placed in air with the neutrons reflecting up to investigate the dry polymer layer or were contained in a heated solid/liquid cell with reflection down geometry to enable potential air bubbles to drift away from the interface (see Figure 2, for the sketch of the experiment). Some measurements were performed using a rheometer (Anton Paar MCR 501) installed *in situ* on the beamline[37] to impose shear stress on the LA film during the passage of the neutron beam. This was done in reflection down geometry, as well. In all cases, a wavelength band between 2 and 20 Å was chosen with a relative wavelength resolution of 3.0% (full width at half-maximum, FWHM). The detector, which allows at the same time the specular and the off-specular reflectivity to be measured, has a resolution of 2.2 × 4.8 mm^2 (FWHM) and a size of 25 × 48 cm^2 at a distance of 2.8 m from the sample. The full *q*-range was obtained with two reflection angles of 0.622 and 2.622°. The beam footprint on the sample was set to 39x39 mm^2 for both reflection angles. The raw data was normalized to the incident beam spectrum by the data reduction software COSMOS.[48]

Ultrathin polymer films on silicon single crystals were first placed in contact with pure D_2O to have a reference state before swelling with BA. These films were then placed in contact with the Pemulen/D_2O mixture containing various fractions of BA in a closed cell. Subsequently, the temperature was increased each 15 min until 70 °C and the structural evolution of the films was observed by NR. Four BA concentrations were studied: 0.3, 0.5, 0.6, and 0.7% BA.

Specular NR Analysis. The measured NR data is subsequently compared to simulated NR curves calculated by an optical matrix formalism from a slab model,[49] and the goodness of the fit is calculated. This least-squares fitting procedure is repeated until convergence is found using MOTOFIT.[50] An alternative fitting program was based on a home modified Refl1D[51] program using python to take into account the relevance of the various parameters of the different models. The model used in all cases consists of an infinitely thick single crystal silicon slab covered by a thin layer of silicon dioxide, whose thickness varied between 1 and 2 nm among the samples, and a layer (or sequence of layers) of swollen LA/D_2O/BA on top capped by an infinite layer of D_2O/BA/Pemulen/TEA.

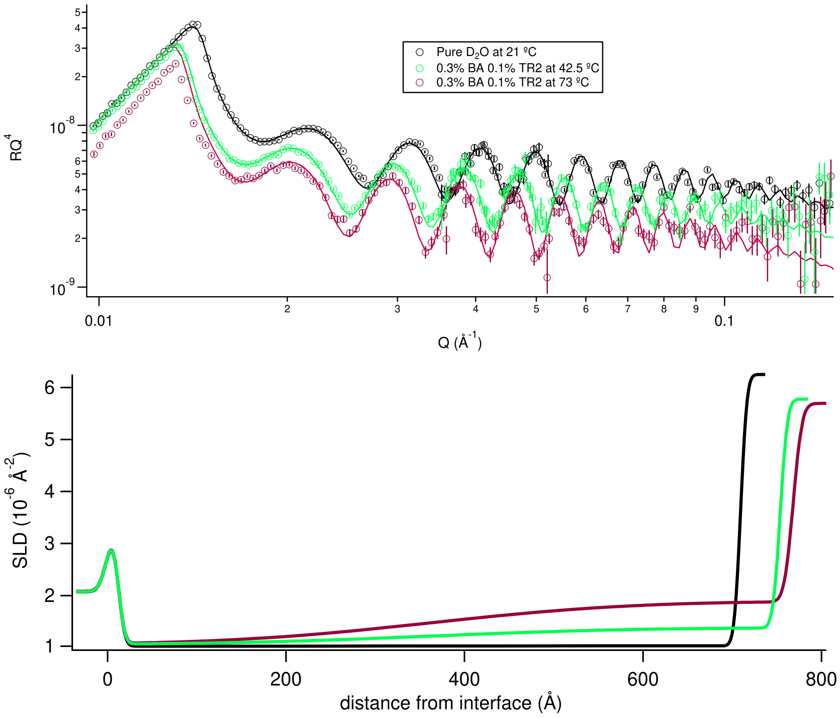

Figure 3. (Top) Typical reflectivity curves (multiplied by q_z^4) vs momentum transfer q_z on a logarithmic scale for LA films in pure D_2O (black circles) and in aqueous solutions of 0.3% BA and 0.1% Pemulen at two different temperatures as depicted in the legend. The solid lines in the same color code are fits to the data. (Bottom) The corresponding SLD profiles in the same color code.

Each of the slabs has three fitting parameters, the thickness, the roughness, and the scattering length density (SLD). The SLD is the number density of isotopes per unit volume multiplied by the corresponding scattering length for neutrons. It can be calculated by knowing the mass density of a material and its chemical sum formula. The SLD calculator from the NIST webpage was used here, which uses tabulated values for scattering lengths and isotope weights.[52] The SLDs and the corresponding chemical sum formulas used in this study can be found in Table S2 in the Supporting Information (SI). The thickness and the roughness of all layers were fitted as well. The silicon substrate and silicon dioxide were found to be atomically smooth (between 0.2 and 0.5 nm) and, therefore, are not discussed further.

Several morphological models were envisaged for the LA layer to fit the data, including (1) a dewetting profile consisting of three sublayers, as shown in Figure 1, dry wetting layer, layer perforated by water-filled holes, and a projected layer due to rims as used in our previous study about the same films in contact with BA/water;[14] (2) LA layers with holes that cross the films down to the substrate without wetting or a rim layer; (3) similar to (2) but with limited depth holes (see Figure 3, bottom); and (4) a single homogeneously mixed layer consisting of LA/BA/water. Note that models (2) and (4) cannot be distinguished by specular reflectometry alone, as for each of these models, the SLD profile is estimated by in-plane averaging the LA and D_2O fractions. The NR spectra were calculated using Motofit or Refl1D with a modified model corresponding to the morphological case and compared to the experimental spectra using a step by step least-squares fitting procedure. To justify the in-plane averaging of the SLDs, the sizes of the defects are supposed to be smaller than the in-plane neutron coherence length.

Note that the scaling of the fitted reflectivity curves was fixed to one in one set of analyses. The lower scaling of the measured curves at an advanced stage of layer destruction is due to enhanced off-specular scattering, as explained in the Supporting Information. In these cases, the low q part of the NR curves was excluded from the fitting procedure. In another set of analyses, the scaling factor was adjusted when the OSS becomes important and the low q part of the NR was also fitted. This analysis strategy led to good fits as well, and the resulting SLD values were not physically reasonable, though.

To extract the partial volume fractions quantitatively from the NR spectra, two approaches were used. First the system was simplified into only two components: a polymer with an $\mathrm{SLD_{LA}}$ value of 0.9×10^{-6} $Å^{-2}$ and a solvent with the fitted $\mathrm{SLD_s}$ values from the critical edge positions of the NR curves. From the fitted mean SLD values, SLD and thicknesses h of the layer, the resulting "dry" volumes of the polymer ν_{pol} (normalized to the dry LA volume), and solvent ν_{s} fractions were extracted using the following formula:

$$\nu_{\mathrm{pol}} = \frac{h(\mathrm{SLD} - \mathrm{SL\ D_s})}{h_0(\mathrm{SL\ D_{LA}} - \mathrm{SL\ D_s})}$$
$$\nu_{\mathrm{s}} = \frac{h}{h_0} - \nu_{\mathrm{pol}} \tag{1}$$

Here, h_0 is the dry thickness of the polymer. This approach does not assume mass conservation but can only extract two unknowns from the two measured values. Assuming conservation of the polymer mass ($\nu_{\mathrm{LA}} = 1$), as done in our previous work for low BA concentrations,[14] one can extract the BA (excess) volume fraction $\phi_{\mathrm{BA/LA}}$ as well as the water fraction $\phi_{\mathrm{W/LA}}$ inside the polymer layer from the following boundary conditions:

$$1 + \phi_{\mathrm{W/LA}} + \phi_{\mathrm{BA/LA}} = \frac{h}{h_0}$$
$$\frac{h}{h_0} {*}\mathrm{SLD} = \phi_{\mathrm{W/LA}} {*}\mathrm{SLD_w} + \phi_{\mathrm{BA/LA}} {*}\mathrm{SLD_{BA}}$$
$$+ (\frac{h}{h_0} - \phi_{\mathrm{W/LA}} - \phi_{\mathrm{BA/LA}}) {*}\mathrm{SLD_{LA}} \tag{2}$$

where $\mathrm{SLD_{BA}}$ is the bulk SLD of BA.

Off-Specular Neutron Reflectivity. As the neutron reflectivity spectra were recorded using two-dimensional (2D) detectors, the off-specular neutron reflectivity (OSS) is also accessible.[53] The OSS intensity corresponds to the intensity scattered at a condition away from the mirror reflection (NR). In this case, the total momentum transfer also comprises an in-plane component. This allows one to determine SLD variations parallel to the interface, but due to the geometry, the momentum transfers are typically 2 orders of magnitude smaller than in specular reflectometry and, therefore, the spatial resolution is much lower probing micrometer-sized structures. The 2D OSS patterns were simulated in wavelength vs scattering angle space using the distorted wave born approximation (DWBA), assuming exponentially decaying in-plane correlation functions.[54] This gave access to one additional parameter, namely, the mean size of in-plane inhomogeneities.

RESULTS

Film Morphology in Contact with BA/TR-2/Water Gel from Specular NR Analysis. A first glance analysis of the NR spectra suggests a substantial LA film swelling in contact with BA/water/Pemulen (Figure 3). In accordance with the previous study, which has shown that the LA thin film dewets the Si substrate when exposed to BA/water mixtures,[14] one could extrapolate this process to explain the NR data in contact with BA/water/Pemulen as well. Dewetting leads to holes and rims and typically yields an averaged SLD profile, as depicted in Figure 1. When, however, the NR spectra of films exposed to BA/water/Pemulen are fitted in terms of this dewetting-induced SLD profile with various rim morphologies (height, width, and fractions), the χ^2 values were found to be minimum for a rim fraction equal to 0 (Figure 4). This strongly rejects rims as a potential morphology in the present case.

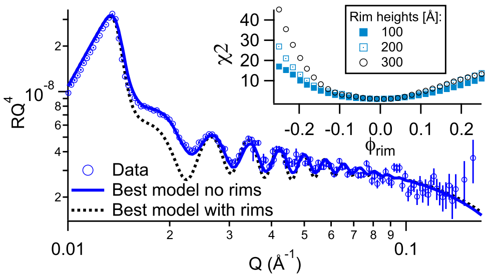

Figure 4. Reflectivity curve (multiplied by q_z^4) vs momentum transfer q_z on a logarithmic scale for a LA film in aqueous solutions of 0.5% BA and 0.1% Pemulen at 27 °C (data points). The solid line in the same color code is the best fit to the data assuming no rims. The broken line is the best fit to the data assuming a rim fraction, as in Figure 1, left. (Inset) Normalized least-squares value χ^2 vs fraction of rims ϕ_{rim} for various heights of rims as indicated in the legend deduced from fitting the specular NR spectra to a model of LA containing a fraction of holes and rims.

The second significant difference compared to LA films immersed in only solvent/nonsolvent mixtures studied previously[14] is the absence of a well-defined wetting layer. Only models of the constant SLD profile or SLD gradients over the entire layer (no sharp SLD step, see Figure 3) lead to reasonable χ^2 values. In all cases, the growth of the average SLD of LA exposed to BA/water/Pemulen is apparent, resulting either from holes that cross the film, noncrossing holes, or heterogeneous zones of LA/BA/water/Pemulen inside the films. All of these models can reasonably fit the specular NR spectra with small variation depending on the fraction of BA and temperature. The best goodness of fit for the 0.3% BA concentration with χ^2 values around 4 was achieved assuming a gradient in SLD across the whole layer starting with the SLD value of the polymer layer when in contact with pure D_2O close to the Si substrate and an increasing SLD toward the aqueous phase. This profile corresponds to a distribution of hole depths with only a few reaching the Si substrate (penetrating the whole film). Typical reflectivity fits and SLD profiles using this model can be seen in Figure 3. For higher BA concentrations, in addition to the gradient, the SLD of the LA in contact with Si had to be fitted as well to reach similar χ^2 values. This resulted in flat SLD profiles inside LA corresponding to water-filled holes crossing the whole film. A typical NR fit, in this case, can be seen in Figure 4.

If the scaling factors of the NR data were adjusted in the fit, qualitatively similar results were obtained, particularly for the total film thickness; however, the absolute SLD values gave nonphysical results.

Effect of Temperature and BA Concentration on Film Swelling in BA/Pemulen/D_2O Gel. Figure 5 shows significant swelling of LA films when exposed to BA/Pemulen/D_2O gels for all of the cases investigated here. For the case of 0.3%, the swelling ratio (SWR) is calculated as the ratio of the film thickness in the presence of BA/Pemulen/water to that in pure D_2O. This is justified by the fact that LA films do not swell in the presence of pure D_2O even after 24 h, at least within the resolution of the NR experiment.[14] At room temperature (21 °C), Figure 5 shows that the LA film swells by 4.5% at a BA concentration of 0.3%, which is the exact same swelling ratio found without the gel.[14] D_2O is unlikely to swell LA films to the extent to be measurable by NR because the Flory−Huggins interaction parameter $\chi_{\text{LA/D}_2\text{O}}$ exceeds 4 at room temperature and, therefore, can safely be excluded as the swelling molecule.[14] LA swelling in BA/Pemulen/D_2O is most likely due to BA, which has a favorable Flory−Huggins interaction parameter $\chi_{\text{BA/LA}}$ between −0.05 and 0.17.[14] Because of its high molecular weight, Pemulen can also be excluded as a swelling agent for LA. Even if TEA can swell LA, it is unlikely to account for the measured LA swelling in the present case because it is highly miscible in water. Even in the extreme case of a similar interaction parameter with water ($\chi_{\text{W/TEA}}$) and LA ($\chi_{\text{LA/TEA}}$), the partitioning of TEA in LA would not exceed the concentration of TEA in water, which is 0.1%, which is within the error bar of the measured SWR.

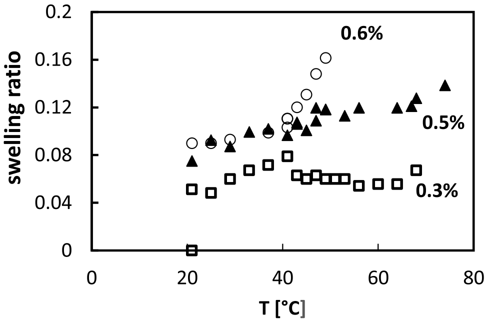

Figure 5. Swelling ratio of a LA film in BA/PTR-2/water vs temperature for the BA fractions of 0.3, 0.5, and 0.6%. The swelling ratio is calculated as the ratio of the film thickness in the presence of BA/PTR-2/D_2O at various temperatures to the initial film thickness in pure D_2O. For 0.5 and 0.6%, the film thickness is extrapolated from the dependence of the swelling ratio on $\phi_{\text{Ba/W}}$ and film thickness at room temperature.

Therefore, one can safely attribute the measured SWR to BA uptake by the LA film.

To extract the individual partitions of the involved materials, the volume fractions of two constituents can be extracted if the polymer mass conservation is not imposed (eq 1) or three constituents if the conservation of polymer mass is assumed (eq 2) from the fitted NR curves with a two-polymer-layer model as described in the Experimental Section. The resulting total volumes of the solvent and polymer within the layer without imposing polymer mass conservation are plotted in Figure 6.

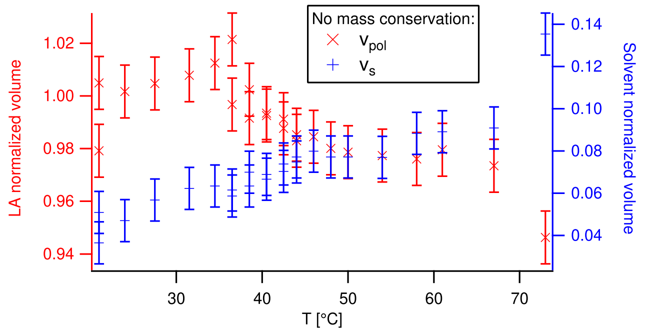

Figure 6. Normalized (excess) volumes of the polymer (red x-crosses, left axis) and liquid (blue crosses, right axis) inside the LA layer from NR of 0.3% BA and 0.1% PTR-2 in D_2O according to the boundary conditions (eq 1) as a function of temperature. Note: the two points at RT for each fraction were measured at two different times, once at the very beginning and a second time after heating to 40 °C, indicating that the polymer loss is irreversible, but the solvent penetration is reversible within error.

As can be seen in the graph, the polymer mass seems to be conserved until 38 °C with an increasing solvent faction with temperature. Above this temperature, there is clearly (irreversible) a loss of polymer observed at the expense of more and more solvent penetrating the film. Therefore, below this temperature, the mass conservation can be assumed and a more detailed partial swelling can be extracted differentiating between water and BA (eq 2). This result is presented in Figure 7.

As suggested above from the Flory–Huggins interaction parameters, indeed, the swelling at RT is mainly attributed to BA with no significant penetration of water. However, with increased temperature (and time), it seems that the volume fractions of both water and BA are increasing. It has to be noted, however, that the increase in the BA fraction with temperature is reversible, but the water fraction increase is not. Therefore, it seems that there are two parameters influencing the partitions: increased chemical compatibility of BA and LA with temperature and onset of dewetting by water-filled cavities with time.

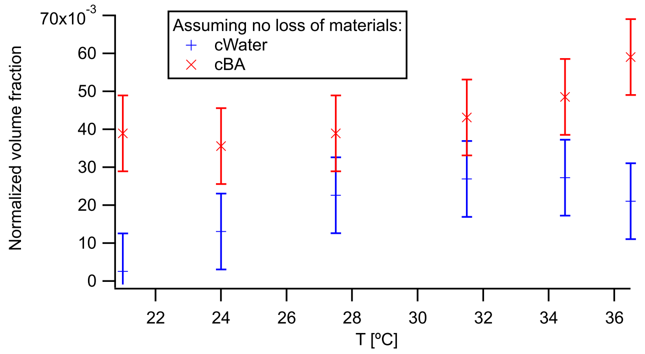

Figure 7. Normalized volume fractions of BA (red x-crosses) and water (blue crosses) from NR of 0.3% BA and 0.1% PTR-2 in D_2O according to the boundary conditions (eq 2) as a function of temperature.

The fact that the presence of hydrophobic domains from the Pemulen TR-2 side group (C10 to C30) does not shift the partitioning balance of BA or water is an important result as Pemulen effectively acts as an emulsifier. This could only infer that the number of hydrophobic moieties at this PTR-2 concentration of 0.1% is not enough to perturb the swelling equilibrium. Recovering the same SWR with or without Pemulen at room temperature for 0.3% is the first important result for restoration processes as this means that there is no need to increase the BA concentration when using Pemulen to control the solvent transfer to the varnish layer, at least when working at room temperature.

Whatever the exact model used for fitting the specular NR of LA in BA/PTR-2/D_2O, an SLD growth with temperature (and time) of the LA film is observed, which can only suggest D_2O invasion into the LA film as it is the largest SLD constituent as quantitatively shown above. The film invasion with water can result either from the creation of penetrating or nonpenetrating holes filled with D_2O or formation of LA/BA/D_2O mixed zones. Assuming holes as the reason for increased water fractions, it is possible to calculate SLD density profiles by assuming a Gaussian distribution of cylindrical water-filled holes around a mean depth inside a LA film of the fitted total thickness. The detailed analysis of the NR spectra with this model assuming LA mass conservation using the least-squares method yields similar tendencies for the dependence of the surface fraction of holes (ϕ_{hole}) on temperature for fully penetrating holes and for holes with finite depth (see Figure 8). ϕ_{hole} was found to increase slightly for 0.3% with increasing the temperature up to 70 °C. On the other hand, ϕ_{hole} for 0.5% strongly increases up to the breaking temperature and for 0.6% increases rapidly from 37 °C up to the breaking temperature of 49 °C. The absolute values of ϕ_{hole} are higher if the LA mass is allowed to decrease, but the qualitative trend stays the same.

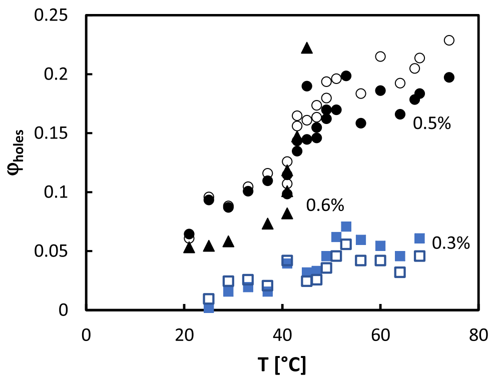

Figure 8. Surface fraction of holes (ϕ_{hole}) containing D_2O vs temperature for films in contact with BA/PTR-2/D_2O for the BA fractions of 0.3, 0.5, and 0.6%. ϕ_{hole} was deduced from fitting the NR spectra to a crossing hole model (full symbols) and noncrossing holes (empty symbols).

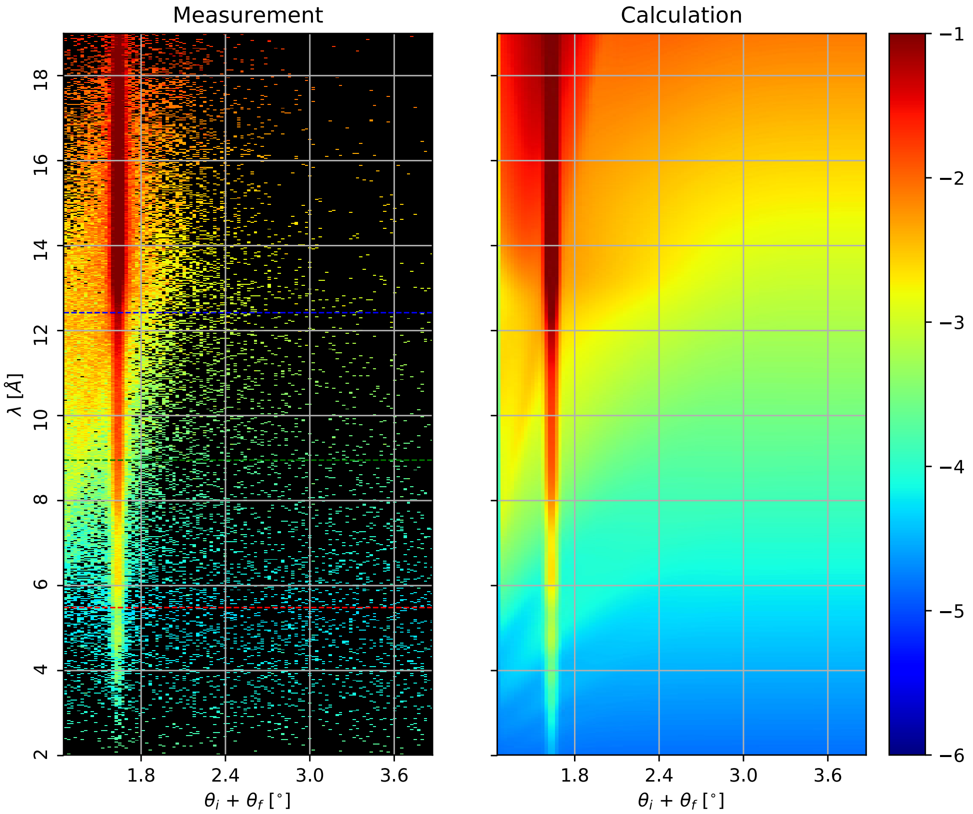

Figure 9. (Left) OSS of a LA film in contact with 0.3% BA and 0.1% PTR-2 in D_2O at 72 °C. (Right) Simulation using the same instrument parameters as in the measurement and using the fitting results from the specular fits and in-plane inhomogeneities filled with water assumed to follow an exponentially decaying SLD on average with a characteristic length of 0.7 μm.

We will therefore present the SLD of the fitted LA layer rather than ϕ_{hole} in the following to be less model dependent.

Effects of Temperature and BA Concentration on the Film Heterogeneities Prior to Film Breaking in the BA/Pemulen/D_2O Dispersion. Many aspects of the reflectivity spectra of Laropal A81 in BA/Pemulen/D_2O point out to the initiation and evolution of significant heterogeneities and defects. This can be seen in the off-specular scattering, film roughness, and the process of water invasion. From the first glance, these defects could be analyzed in terms of a simple dewetting process induced by BA, as in the case BA/D_2O (without Pemulen). However, significant morphological differences to the case in pure water are observed and will be discussed in the following.

Film Heterogeneities from OSS. In all NR measurements, a clear Yoneda-type scattering was observed around the critical momentum transfers (see Figure 9). This points toward in-plane SLD correlations present in the system. Quantitative fits of the 2D scattering patterns[54] clearly showed that the origin of this scattering comes from inhomogeneities inside the bulk of the film filled with water. The interface roughness as the only origin of the scattering can be clearly excluded as this would lead to much less scattered intensity. Moreover, it became evident that the SLD contrast contributing to this scattering must come from D_2O rich phases inside the polymer, which is the largest SLD contrast when looking at Table S2 in the Supporting Information. This shows striking similarities to our previous study of LA films in binary water/BA mixtures,[14] where water-filled holes were the origin of the OSS scattering as evidenced by AFM. In the present case, AFM measurements were not possible as the gelly solution was sticking to the polymer films and impossible to be removed without detachment of the LA film as well.

From the quantitative fits of the OSS intensity to an exponentially decaying in-plane SLD inhomogeneity, one can extract a characteristic in-plane correlation length, which would correspond to an average hole radius in the case of holes. This is plotted in Figure 10 for a 0.5% BA solution in 0.1% Pemulen as a function of temperature. In addition, the SLD from the specular fits is shown on the same graph. To put these results into perspective with the pure water case, the results from a similar LA film in contact with a 0.5% BA solution in pure water are added to the graph. These are from the preceding

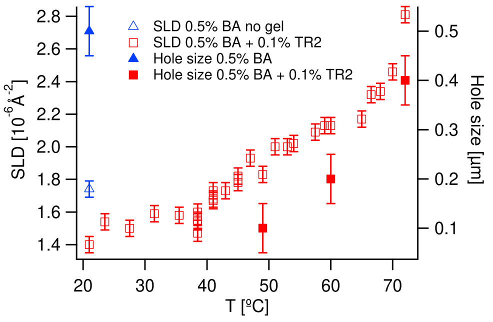

Figure 10. (Left axis) SLD as a function of temperature from a LA polymer film in contact with 0.5% BA and 0.1% PTR-2 in D_2O (open squares). (Right axis) Extracted hole radius from the OSS simulations of the same sample (filled squares). The triangles correspond to the SLD (open triangle) and the hole radius (filled triangle) of a LA film in contact with a 0.5% BA solution in pure D_2O after 2 h immersion.

study done at room temperature only.[14] Here, another apparent difference between the varnish in contact with a gel and with pure water, both containing BA, can be appreciated. While the SLD is on the same order for both cases at low temperatures, it clearly increases significantly for the gelly case at elevated temperatures. The SLD increase is linearly related to the volume fraction of water-filled holes inside the layer, which means that the volume fraction of holes is significantly higher in the Pemulen solution at elevated temperatures compared to the pure water case at RT. On the other hand, the size of the holes is smaller in the case of the polymer dispersion, even at the highest temperature investigated here. This unambiguously testifies a significantly higher hole density in the case of the Pemulen solution. Assuming the hole size extracted from the quantitative OSS fits to be the hole radius, the hole density at RT for 0.5% BA in pure water is about 0.1 μm^{-2} and for the same BA concentration inside the Pemulen solution at 49 °C is about 3 μm^{-2} if the holes are not overlapping.

Interface between Varnish Films and PTR-2/BA Aqueous Solutions. The microscopic roughness of the polymer/liquid interface deduced from NR analysis is found to be around 0.6 nm at room temperature and low BA concentrations, while increasing to up to 1.2 nm at higher temperatures or BA concentrations. These values are manifestly higher than the reported one in the case of the binary BA/D_2O mixture,[14] which never exceeded 0.3 nm. This suggests that adding Pemulen into the aqueous phase favors surface roughness.

An immiscible polymer/polymer interface should develop an interface width σ corresponding to the squared sum of the intrinsic roughness σ_i coming from chemical interactions and scaling with the monomer size a,[55] and the capillary wave roughness σ_{CW} due to interfacial tension γ if the sample is in equilibrium[56]

$$\sigma^2 = \frac{k_B T}{2\pi\gamma} \ln\left(\frac{l_c}{a}\right) + \sigma_i^2 \tag{3}$$

where the capillary wave spectrum is cut by the neutron coherence length l_c. k_B denotes the Boltzmann constant. The intrinsic width for a high Flory−Huggins interaction parameter χ can be estimated by[55]

$$\sigma_i = \frac{a\sqrt{N}}{3\sqrt{\chi/2^*N - 1}} \tag{4}$$

with the polymerization N. The surface energy of Laropal A81 was determined by measuring the contact angle of different liquids on top of a macroscopic LA film[57] and turned out to be around 30 mN/m.

Using water as the "monomer" with a typical size of a water molecule of 1.8 Å,[58] one gets indeed around 3 Å, the roughness of the interface using the χ values between 2.5 and 4 and N = 30 as determined in our previous study.[14] Using around 1 nm as the size of the monomer results in roughness between 4.5 and 5.5 Å, for the binary mixture. In the case of the lower surface tension of the gelled solvent of around 56 mN/m,[32] we indeed get higher values between 3.6 and 5.9 Å, using 1.8 Å or 1 nm as the monomer size, respectively, assuming the same χ values as for the binary mixtures. This slight roughness increase can explain the interface width of the polymer/D_2O/Pemulen system measured at RT, which is around 6 Å, for 0.3 or 0.5% BA, especially taking into account that Pemulen acts as an emulsifier, although its volume fraction is very low (0.1%). The increase of the roughness with temperature up to 70° between 1 and 2 Å, for the 0.3 or 0.5% BA mixtures, respectively, is, however, more than what would be expected by a mere reduction in interfacial tension with increasing temperature. Moreover, the roughness values above 1 nm in the case of 0.6% BA cannot be explained by a decreased interfacial tension alone, but have to involve a reduction of the Flory−Huggins interaction parameter as a function of temperature. This result is in accord with the increased BA swelling of LA at elevated temperatures as observed in Figure 7.

Interestingly, the temperature-induced roughness increase of the aqueous/polymer interface seems to plateau at a certain temperature, as can be seen in Figure 11. The origin of this effect remains somewhat unclear. This temperature is close to the glass transition temperature if calculated using the binary mixing model, as will be explained later. One could therefore imagine that "unfreezing" of stress could be the origin of this stagnation. Note, however, that the change in roughness is reversible as the value at room temperature was measured twice at different moments during the heating protocol (see the two points at RT in Figure 11). Therefore, this behavior is unlikely to be related to nonequilibrium properties. On the other hand, starting from 40 °C, a loss of polymer mass is observed (see Figure 6) by the formation of water-filled cavities. It is therefore possible that the roughness contribution due to these cavities is significantly larger than the intrinsic interface roughness and, therefore, screens the latter as specular NR measures only the sum of the two contributions. Again, the reversibility of the roughness increases even after the appearance of cavities contradicts this hypothesis. Another possibility is that the interaction between BA and LA becomes athermal above 40 °C, meaning no further improvement of the polymer/solvent compatibility at higher temperatures. A counter indication to this explanation is that in a test, a LA/BA mixture (5% BA) was cooled down to −20° and showed no indication of phase separation, meaning that the BA at room temperature is already far away from theta conditions, also consistent with the very low Flory−Huggins parameter around 0.

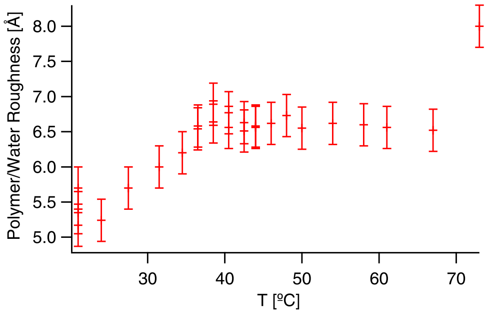

Figure 11. Roughness of the aqueous/polymer interface deduced from NR for a solution of 0.3% BA and 0.1% PTR-2 in D_2O as a function of temperature.

Finally, the roughening of the polymer/liquid interface could also be attributed to the presence of TEA. The presence of weak surface-active molecules might help the formation of interfaces, increasing the actual roughness or leading to a larger SLD gradient upon adsorption, visible as an increased interface roughness (rather than a distinct layer) due to the small size of TEA.

For higher BA concentrations, the roughness values are generally higher, going up to 1.2 nm, but show a similar increasing trend with temperature. Due to the limited temperature ranges available for the other BA concentrations and larger uncertainties, their trends are not obvious and, therefore, they were not analyzed further.

Temperature and Solvent Influence on the Stability of the Film. An important outcome of this experiment regarding the art restoration field is the onset of film breaking and destruction. Indeed, while increasing the temperature, most of the films investigated here, except for 0.3%, breaks within the NR experiment, yielding nonquantifiable NR spectra. The critical temperature (T_{crit}) for film breaking is found to be BA fraction-dependent and decreases with increasing BA from room temperature to above 72 °C (Figure 12). At 0.3%, the film never breaks until the temperature limit of this study (16.5−73 °C). At 0.5%, the temperature of the film breaking was 72 °C, at 0.6% BA at 44 °C, and at 0.7% BA only at 21 °C.

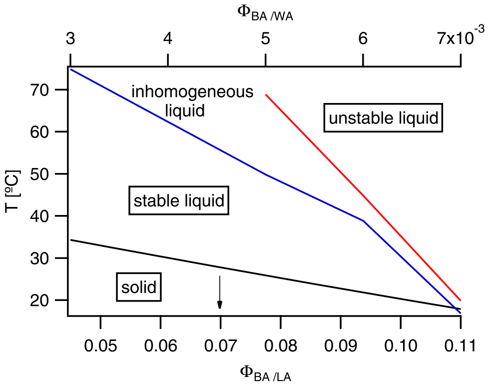

Figure 12. Film stability diagram using the T_g and NR results. The lower black line corresponds to the T_g as calculated from eq 5 using the BA in LA volume fractions from the bottom axis. The blue line in the middle corresponds to the threshold temperature where the OSS intensity is 10^4 counts per minute in Figure S4 from the SI and the red line in the upper right corner marks the temperature at which a sudden loss of most of the film's material is observed. The latter two lines relate to the upper x-axis (BA fraction in water) and are deduced from the experimental data.

The basic idea behind the strategy of adding moieties of good solvent to a bad solvent gel in art restoration is softening the varnish film to promote its mechanical removal by abrasion. This would lead to reducing its T_g below room temperature via solvent plasticizing. The results presented here show that the mechanism is more complex, and the chemical interaction plays an important role in this process.

The T_g of the binary LA/BA mixture can be estimated using the partitioning constant of BA between LA and water from NR experiments on thin films[14] and the mixing model

$$\frac{1}{T_g} = \frac{1 - \phi_{BA}}{T_{g(LA)}} + \frac{\phi_{BA}}{T_{g(BA)}} \qquad (5)$$

using $T_{g(BA)} = -105.15$ °C[59] for BA and $T_{g(LA)} = 47$ °C for LA, and the $\phi_{BA/LA}$ concentrations from our previous study.[14] The resulting glass transition temperature as a function of $\Phi_{BA/WA}$ is plotted in Figure 12 as a black line and decreases from around 35 °C at 0.3% BA to 18 °C at 0.7% BA, the highest solvent concentration examined in this study. The temperature at which a sudden increase in mass loss is observed (film removal) is at 44 °C for 0.6% BA, 72 °C for 0.5% BA, and above 72 °C for 0.3% BA, which is 20−37 °C above the respective glass transition temperature. This suggests that the sudden unfreezing of the film's surface tension stress is not the main motor for film breaking because at 0.3 and 0.5% BA concentrations, the film remains largely intact. This does not mean, however, that residual stress cannot be the origin of hole nucleation, as observed for other polymer thin films.[60]

Another important outcome of the fact that the film remains largely intact for extended periods of time more than 20 °C above T_g is that the kinetics driving the film destruction are not controlled by the polymer viscosity. As LA is a low molecular weight polymer, its viscosity should decrease by orders of magnitude when crossing T_g. If "normal" dewetting, whose kinetics are governed by viscosity, was to be the origin of film destruction in the here studied case, the kinetics should accelerate by orders of magnitude above T_g as observed with thin polystyrene film dewetting from functionalized silicon substrates. An acceleration of a factor 10 was observed when heating the sample by 10 °C above T_g.[61] In the case studied here, the polymer film in contact with a copolymer solution containing 0.3% BA was withstanding more than 10 h at temperatures significantly above T_g, showing a clear layered structure observed by Kiessig fringes in the NR curves despite a high fraction of holes present. If, on the other hand, the BA concentration in the solution is increased to 0.7%, the film is almost completely lost within only 3.5 h at 19 °C, which is around T_g. In essence, clearly, the BA concentration inside the polymer is driving the kinetics of film destruction and not the polymers' viscosity.

The fact that the polymer softening is not the main driver for film break-up can also be appreciated by the concentration and temperature dependence of the different stages of film destruction. In Figure 12, the information from T_g estimations, specular and off-specular NR on the state of the varnish film, is summarized in a film stability diagram. The boundaries in this diagram are chosen to separate three regimes of film stability depending on $\phi_{BA/W}$ and temperature. (a) The area below the black line corresponds to the solid zone below T_g as calculated from eq 5. (b) At higher temperatures, the polymer is liquid but does not show pronounced hole formation as evidenced by low OSS intensity. It is chosen to separate this phase from the inhomogeneous zone at higher temperatures by a threshold of Yoneda peak intensity of 10^4 counts per minute (see Figure S4 in the Supporting Information), marked by a blue line. This choice is arbitrary, but its exact value will only shift the temperature of the boundary keeping the qualitative behavior with the BA concentration the same. Finally, the red line marks the temperature at which a sudden loss of most of the film's material is observed.

Looking at this film stability diagram, it is obvious that the boundaries of film destabilization are uncorrelated with the T_g evolution. While T_g is decreasing almost linearly with the BA concentration in the investigated range with a rather small slope, the other boundaries show a much steeper BA dependence and are not necessarily linear.

■ DISCUSSION

Given the clear indications that the appearance of water-filled holes growing with time is responsible for the here studied film destruction, dewetting might seem to be the most likely scenario. Moreover, a very similar behavior of the scattering curves at the late stages of film destruction, compared to the case of pure water where dewetting was observed, can be shown as evidenced in the Supporting Information. Clearly, the driving force is the hydrophilicity of the used substrate attracting the polar emulsifier and/or water, as observed in our previous study.[14] The role of polar forces in dewetting of thin hydrophobic polymer films was also shown for polystyrene supported by silicon wafers immersed in poor solvents[30] or nonsolvent/poor solvent mixtures.[31]

However, several contradictions to the process of dewetting are observed. The most significant one is probably the fact that the kinetics are not governed by the polymer viscosity, but linked to the amount of solvent swelling. Clearly, the retardation of dewetting is gradually switched off by increased solvent concentration inside the polymer. Suppression of dewetting was already observed for thin polystyrene films when their chain ends were functionalized by polar groups, explained by their bonding to the polar substrate and between the chains stabilizing the film.[29] Laropal is known to incorporate a significant amount of polar groups as well,[40] and in our previous study of LA films in contact with water/BA mixtures, we observed a wetting layer that was not perforated by the dewetting holes testifying the strong bonding of annealed LA to the polar substrate.[14] However, at higher BA concentrations or longer exposure, the vast majority of the film vanished, eventually. In the aforementioned study, we also observed a retarded swelling of the LA film when exposed to aqueous solutions containing increasing amounts of BA. While for small solvent concentrations almost no swelling was observed, a linear swelling behavior was recovered as predicted for bulk LA at BA concentrations above 0.2%. We argued that bonding or cross-linking of some sites of the polymer to the substrate was responsible for this swelling retardation, which would be gradually suppressed by the addition of BA.

It is possible that a similar mechanism is at play in the here studied case of the same LA film in contact with a BA containing viscous polymer dispersion. Indeed, for 0.3% BA we again observe a quasi-water-free zone close to the substrate (see Figure 3, bottom), although this "wetting layer" is much less pronounced compared to our previously investigated case without Pemulen. In addition, contrary to our previous study, at higher BA concentrations, this dry layer is not visible anymore. This could be, however, due to the much more polar −OH groups contained in the copolymer in comparison to water. Therefore, the scenario of dewetting retardation due to polar group interactions inside the polymer film and with the polar substrate, which is gradually screened or broken by the polar BA seems to be the most likely scenario. The highly stable film state could also be appreciated by a test where *in situ* shear was applied to the BA swollen film, not altering its structure, as shown in the Supporting Information.

Another contradiction with typical dewetting (and the previous study on binary water/solvent systems) is the here observed absence of rims. However, this could be explained by (a) the fact that the polymer/substrate interaction is effectively weaker due to the presence of highly charged groups of Pemulen, similar to the absence of rims observed for films experiencing plug flow,[62] (b) the smaller size of holes, similar to the early stages of dewetting of polymer films on nonadsorbing substrates,[28] or most importantly (c) the fact that the films are effectively fluid, being above the T_g while the dewetting speed is retarded and, thus, not limited by viscosity, giving the films the time to reach their equilibrium thickness at any stage of dewetting.

Due to the presence of an emulsifier in the system (Pemulen TR-2), we cannot exclude gradual emulsification of the LA film by its incorporation into the aqueous phase due to the hydrophobic side groups of Pemulen, leaving behind voids and leading to holes in the film. Due to the high viscosity of the solution, it is technically challenging to establish an equilibrium phase diagram of the here studied system in contrast to the water-based system studied before.[14] However, Pemulen TR-2 is known to form a microgel with typical droplet sizes in the (sub-)micron range when stabilizing an emulsion.[33] Therefore, an emulsification process starting from the polymer/gel interface should engender a significant roughening of the polymer surface. As seen in Figure 11, the measured polymer film roughness for a BA concentration of 0.3% never exceeds 1 nm testifying to a molecularly smooth layer just before film rupture.

We note that the amount of benzyl alcohol inside the Pemulen solution was up to 0.7% in the current study, which is significantly lower than the solubility limit in water (4%). We therefore expect the solvent to be homogeneously distributed as is the case in pure water.

Finally, the presence of TEA being a weak surface-active molecule might help the formation of interfaces and intermediate steps in the first stages of dewetting, kinetically favoring the process, leading to the observed higher coverage of smaller holes.

On an application level, the results of this paper, such as the presence of holes or the temperature effect, provide new information for painting conservators and restorers. In case the holes pierce the entire varnish layer, the penetration of the solvent contained in the Wolbers gel can reach and get into the paint layer. Thus, inducing an irreversible risk of deformation, swelling, and dissolution of this fragile layer. The appearance of (sub-)micron-sized holes would also reduce the transparency of the coating. It has to be noted, however, that the here used silicon substrate is slightly hydrophilic and, thus, not generally representative for the pictorial layer supporting the varnish, being typically hydrophobic. Nonetheless, deeper layers in an easel painting can be hydrophilic due to the glue typically used to support the preparation. This could be exposed to the varnish in cases of cracks. Another difference in real paintings is of course the absence of sharp boundaries between the layers. These gradual boundaries have a stabilizing effect on film cohesion.

On the other hand, the results of the combined action of temperature and solvent show that it is possible to remove varnish without mechanical stress, as is currently the case. Now, restorers have a better understanding of the process of removing varnish from paintings using solvent-loaded gels and can re-evaluate this approach to guarantee the safety of the paint layer.

■ CONCLUSIONS

The above results on the destruction of Laropal A81 films in contact with a solvent containing viscous polymer dispersions clearly show striking similarities with binary solvent/non-solvent mixtures studied earlier,[14] which points toward a dewetting-type process in the here studied system as well. As in the former case, the appearance of water-filled cavities in the film is initiated by the addition of a good solvent and significantly accelerated if the amount of solvent is increased.

An increase in temperature above T_g, in turn, is not accelerating the dewetting kinetics as much, clearly showing that the dewetting speed is not viscosity limited as it is the case for pure nonpolar polymers pointing toward a retardation of film destruction as seen for polymers having polar groups incorporated.[29] It is argued that the addition of polar solvent is screening or breaking the polar interactions inside the film and/or with the polar substrate, leading to accelerated film destruction. Another similarity to the pure water case is the loss of polymer mass at the late stages of dewetting.

There are, however, significant differences in the here studied case of a gelly matrix in comparison to the dewetting of Laropal A81 in binary mixtures. No rims are observed, no clear wetting layer is seen, and the size of the holes is significantly smaller, although their volume fraction is similar inside the layer. The smaller size of the holes and thus larger hole density can be explained by an increased spreading coefficient of the gel on the Si substrate due to the presence of highly charged −OH groups from the gel. It was shown that the hole density in dewetting polystyrene films on treated Si substrates is larger when in contact with higher energy surfaces.[63] The smaller size of the holes in turn partially explains why no rim is visible as the rim is not present for holes at the early stages of viscoelastic film dewetting from nonadsorbing substrates.[28,64] In this case, the altered interaction at the polymer/solid interface could also be the reason why no wetting layer is observed. Another explanation for the absence of rims could be the fluid nature of the film as the dewetting speed is obviously not viscosity limited.

In summary, the destruction of LA varnish films as used in art restoration when in contact with Pemulen TR-2 aqueous solutions containing small amounts of solvent is not principally driven by the reduction of the polymer's T_g but clearly governed by the good solvent swelling. The destruction is clearly occurring by the appearance of water-filled holes, similar to the previously reported dewetting-type process of the same films in binary solvent/nonsolvent mixtures. Obviously, this behavior would be catastrophic for art restoration, it has to be noted, though, that the here used support (silicon) is hydrophilic, while the surfaces supporting the protective varnish layers in easel paintings are typically hydrophobic. However, the presence of polar groups inside Laropal A81 seems to play a determining role for film stability, which is gradually screened by the addition of the polar solvent. This brings to evidence the importance of polar interactions in LA film removal, which should be taken into account in restoration recipes.

The presence of the gellifying polymer, however, apparently changes the interface width between the varnish and the polymer solution without shifting the solvent partition in the bulk of the materials. This opens a way for art restoration to tune the chemical and surface interactions, not only by varying the concentrations of the involved materials but notably by changing temperature. This is potentially a way to make varnish removal safe for art restoration by the use of gels in a temperature-controlled way. The smaller size of the holes can also be less evident concerning optical distortions.

■ ASSOCIATED CONTENT

Supporting Information

The Supporting Information is available free of charge at https://pubs.acs.org/doi/10.1021/acs.langmuir.0c02162.

Additional NR fitting results; precharacterization of LA layers; comparison of NR and OSS between LA films in contact with gel and pure water containing high BA concentrations and additional optical micrographs of LA films after long exposure to pure water and BA; and *in situ* Rheo-NR of BA swollen LA films in contact with gel + BA (PDF)

■ AUTHOR INFORMATION

Corresponding Authors

Philipp Gutfreund − *Large Scale Structures Group, Institut Laue-Langevin, Grenoble 38000, France;* orcid.org/0000-0002-7412-8571; Email: gutfreund@ill.fr

Yahya Rharbi − *Laboratoire de Rhéologie et Procédés, Grenoble 38000, France*; Email: yahya.rharbi@univ-grenoble-alpes.fr

Authors

Amélie Castel − *Large Scale Structures Group, Institut Laue-Langevin, Grenoble 38000, France; Laboratoire de Rhéologie et Procédés, Grenoble 38000, France*

Bernard Cabane − *ESPCI Paris Tech, Paris 75005, France*

Complete contact information is available at: https://pubs.acs.org/10.1021/acs.langmuir.0c02162

Notes

The authors declare no competing financial interest.

■ ACKNOWLEDGMENTS

We thank the ILL for neutron beam time on FIGARO (doi.ill.fr/10.5291/ILL-DATA.1-03-36). We thank the Partnership for Soft Condensed Matter at ILL for the use of complimentary techniques. The Laboratoire de Rhéologie et Procédés is part of the LabEx Tec 21 (Investissements d'Avenir—grant agreement no ANR-11-LABX-0030) and of the PolyNat Carnot Institut (Investissements d'Avenir—grant agreement no ANR-11-CARN-030-01). The open access fee was covered by FILL2030, a European Union project within the European Commission's Horizon 2020 Research and Innovation programme under grant agreement N°731096.

■ REFERENCES

(1) Debnath, K.; Bucio, T. D.; Al-Attili, A.; Khokhar, A. Z.; Saito, S.; Gardes, F. Y. Photonic crystal waveguides on silicon rich nitride platform. *Opt. Express* **2017**, *25*, 3214−3221.

(2) Crudden, C. M.; Horton, J. H.; Narouz, M. R.; Li, Z.; Smith, C. A.; Munro, K.; Baddeley, C. J.; Larrea, C. R.; Drevniok, B.; Thanabalasingam, B.; et al. Simple direct formation of self-assembled N-heterocyclic carbene monolayers on gold and their application in biosensing. *Nat. Commun.* **2016**, *7*, No. 4481.

(3) Teh, L.; Tan, N.; Wong, C.; Li, S. Growth imperfections in three-dimensional colloidal self-assembly. *Appl. Phys. A* **2005**, *81*, 1399−1404.

(4) Boissière, C.; Grosso, D.; Prouzet, E. Inorganic Nanomaterials Synthesis Using Liquid Crystals. In *Encyclopedia of Inorganic Chemistry*; Wiley, 2006.

(5) Stolow, N. Action of solvents on dried linseed oil films. *Nature* **1957**, *179*, 579.

(6) Stolow, N. The measurement of film thickness and of solvent action on supported films. *Stud. Conserv.* **1957**, *3*, 40−44.

(7) Michalski, S. A physical model of the cleaning of oil paint. *Stud. Conserv.* **1990**, *35*, 85−92.

(8) Phenix, A.; Sutherland, K. The cleaning of paintings: effects of organic solvents on oil paint films. *Stud. Conserv.* **2001**, *46*, 47−60.

(9) Fife, G. R.; Stabik, B.; Kelley, A. E.; King, J. N.; Blümich, B.; Hoppenbrouwers, R.; Meldrum, T. Characterization of aging and solvent treatments of painted surfaces using single-sided NMR. *Magn. Reson. Chem.* **2015**, *53*, 58−63.

(10) Brandi, C.; Déroche, C. *Théorie de la restauration*; École nationale du patrimoine, 2001.

(11) Stolow, N. Application of science to cleaning methods: Solvent action studies on pigmented and unpigmented linseed oil films. *Stud. Conserv.* **1961**, *6*, 84−88.

(12) Graham, I. The effect of solvents on linoxyn films. *F. Oil Col* **1953**, *36*, 500.

(13) Carretti, E.; Bonini, M.; Berrie, L. D. B.-H.; Angelova, L.-V.; Baglioni, P.; Weiss, R.-G. New frontiers in Materials Science for Art Conservation: Responsive Gels and Beyond. *Acc. Chem. Res.* **2010**, *43*, 751−760.

(14) Castel, A.; Gutfreund, P.; Cabane, B.; Rharbi, Y. Swelling, dewetting and breakup in thin polymer films for cultural heritage. *Soft Matter* **2020**, *16*, 1485−1497.

(15) Wolbers, R. *Cleaning Painted Surfaces: Aqueous Methods*; Archetype: London, 2000.

(16) Bertolucci, S.; Bianchini, E.; Biave, C.; Caliari, F.; Cremonesi, P.; Gravina, S.; Zammataro, M.; Zangani, B. Preparazione e utilizzo di soluzioni acquose addensate, reagenti per la pulitura di opere policrome. *Progetto restauro* **2001**, *7*, 28−33.

(17) Sun, M.; Zou, J.; Zhang, H.; Zhang, B. Measurement of reversible rate of conservation materials based on gel cleaning approach. *J. Cult. Heritage* **2015**, *16*, 719−727.

(18) Guizzo, S.; Tortolini, C.; Pepi, F.; Leonelli, F.; Mazzei, F.; Di Turo, F.; Favero, G. Application of microemulsions for the removal of synthetic resins from paintings on canvas. *Nat. Prod. Res.* **2016**, 1−11.

(19) Rodriguez, S. H. *Les propriétés, actions et principales problématiques des gels de Pemulen TR-2. Le choix de la base dans la formulation des gels*; CeROArt: Conservation, exposition, Restauration d'Objets d'Art, 2017.

(20) Salama, K. K.; Ali, M. F.; El-Sheikh, M. S. The Conservation of an Egyptian Coptic Fresco Painting from Saint Jeremiah Monastery: The Use of Nano-Materials in Cleaning and Consolidation. *J. Nano Res.* **2017**, 148−153.

(21) Baglioni, P.; Berti, D.; Bonini, M.; Carretti, E.; Dei, L.; Fratini, E.; Giorgi, R. Micelle, microemulsions, and gels for the conservation of cultural heritage. *Adv. Colloid Interface Sci.* **2014**, *205*, 361−371.

(22) Chelazzi, D.; Giorgi, R.; Baglioni, P. Microemulsions, micelles, and functional gels: how colloids and soft matter preserve works of art. *Angew. Chem., Int. Ed.* **2018**, *57*, 7296−7303.

(23) Singh, A.; Mukherjee, R. Swelling Dynamics of Ultrathin Polymer Films. *Marcomolecules* **2003**, *36*, 8728−8731.

(24) Miller-chou, B.-A.; Koenig, J.-L. A review of polymer dissolution. *Prog. Polym. Sci.* **2003**, *28*, 1223−1270.

(25) Ellison, C.-J.; Torkelson, J.-M. The distribution of glass-transition temperatures in nanoscopically confined glass formers. *Nat. Mater.* **2003**, *2*, 695−701.

(26) Nieto Simavilla, D.; Huang, W.; Housmans, C.; Sferrazza, M.; Napolitano, S. Taming the Strength of Interfacial Interactions via Nanoconfinement. *ACS Cent. Sci.* **2018**, *4*, 755−759.

(27) Seemann, R.; Herminghaus, S.; Neto, C.; Schlagowski, S.; Podzimek, D.; Konrad, R.; Mantz, H.; Jacobs, K. Dynamics and structure formation in thin polymer melt films. *J. Phys.: Condens. Matter* **2005**, *17*, S267−S290.

(28) Reiter, G. Dewetting of highly elastic thin polymer films. *Phys. Rev. Lett.* **2001**, *87*, No. 186101.

(29) Henn, G.; Bucknall, D. G.; Stamm, M.; Vanhoorne, P.; Jérôme, R. Chain End Effects and Dewetting in Thin Polymer Films. *Macromolecules* **1996**, *29*, 4305−4313.

(30) Xu, L.; Sharma, A.; Joo, S. W. Dewetting of Stable Thin Polymer Films Induced by a Poor Solvent: Role of Polar Interactions. *Macromolecules* **2012**, *45*, 6628−6633.

(31) Xu, L.; Sharma, A.; Joo, S. W.; Liu, H.; Shi, T. Unusual Dewetting of Thin Polymer Films in Liquid Media Containing a Poor Solvent and a Nonsolvent. *Langmuir* **2014**, *30*, 14808−14816.

(32) Simovic, S.; Tamburic, S.; Milic-Askrabic, J.; Rajic, D. An investigation into interactions between polyacrylic polymers and a non-ionic surfactant: an emulsion preformulation study. *Int. J. Pharm.* **1999**, *184*, 207−217.

(33) Szűcs, M.; Sandri, G.; Bonferoni, M. C.; Caramella, C. M.; Vaghi, P.; Szabó-Révész, P.; Erős, I. Mucoadhesive behaviour of emulsions containing polymeric emulsifier. *Eur. J. Pharm. Sci.* **2008**, *34*, 226−235.

(34) Feller, R.-L.; Stolow, N.; Jones, E.-H. *On Picture Varnishes and Their Solvents*; Revised and Enlarged edition; Works, A., Eds.; National Gallery of Art Distributed by The Foundation of the American Institute for Conservation of Historic, 1971.

(35) Diethert, A.; Metwalli, E.; Meier, R.; Zhong, Q.; Campbell, R.-A.; Cubitt, R.; Müller-Buschbaum, P. In situ neutron reflectometry study of the near-surface solvent concentration profile during solution casting. *Soft Matter* **2011**, *7*, 6648−6659.

(36) Michalski, S. A physical model of the cleaning of oil paint. *Stud. Conserv.* **1990**, *35*, 85−92.

(37) Wolff, M.; Kuhns, P.; Liesche, G.; Ankner, J. F.; Browning, J. F.; Gutfreund, P. Combined neutron reflectometry and rheology. *J. Appl. Crystallogr.* **2013**, *46*, 1729−1733.

(38) https://www.basf.com.

(39) de la Rie, E. D.; Lomax, S.; Palmer, M.; Glinsman, L.; Christopher, A. An investigation of the photochemical stability of urea-aldehyde resin retouching paints. *Stud. Conserv.* **2000**, *45*, 51−59.

(40) Bonaduce, I.; Colombini, M.; Degano, I.; Girolamo, F. D.; Nasa, J. L.; Modugno, F.; Orsini, S. Mass spectrometric techniques for characterizing low-molecular-weight resins used as paint varnishes. *Anal. Bioanal. Chem.* **2012**, *405*, 1047−1065.

(41) Maines, C. A.; la Rie, E. D. Size-exclusion chromatography and differential scanning calorimetry of low molecular weight resins used as varnishes for paintings. *Prog. Org. Coat.* **2004**, *52*, 39−45.

(42) http://www.ctseurope.com.

(43) Madsen, F.; Eberth, K.; Smart, J. D. A rheological assessment of the nature of interactions between mucoadhesive polymers and a homogenised mucus gel. *Biomaterials* **1998**, *19*, 1083−1092.

(44) Ravenel, N. Pemulen TR-2: An Emulsifying Agent with Promise. *WAAC Newsl.* **2010**, *32*, 10−12.

(45) Shahin, M.; Hady, S. A.; Hammad, M.; Mortada, N. Optimized formulation for topical administration of clotrimazole using Pemulen polymeric emulsifier. *Drug Dev. Ind. Pharm.* **2011**, *37*, 559−568.

(46) Hall, D. B.; Underhill, P.; Torkelson, J. M. Spin coating of thin and ultrathin polymer films. *Polym. Eng. Sci.* **1998**, *38*, 2039−2045.

(47) Campbell, R. A.; Wacklin, H. P.; Sutton, I.; Cubitt, R.; Fragneto, G. FIGARO: The new horizontal neutron reflectometer at the ILL. *Eur. Phys. J. Plus* **2011**, *126*, No. 329.

(48) Gutfreund, P.; Saerbeck, T.; Gonzalez, M. A.; Pellegrini, E.; Laver, M.; Dewhurst, C.; Cubitt, R. Towards generalized data reduction on a chopper-based time-of-flight neutron reflectometer. *J. Appl. Crystallogr.* **2018**, *51*, 606−615.

(49) Abelès, F. Recherches sur la propagation des ondes électromagnétiques sinusoïdales dans les milieux stratifiés-Application aux couches minces. *Ann. Phys.* **1950**, 596−640.

(50) Nelson, A. Co-refinement of multiple-contrast neutron/X-ray reflectivity data using MOTOFIT. *J. Appl. Crystallogr.* **2006**, *39*, 273−276.

(51) https://refl1d.readthedocs.io/en/latest/.

(52) https://www.ncnr.nist.gov/resources/activation/.

(53) Lauter, V.; Lauter, H.; Glavic, A.; Toperverg, B. *Reference Module in Materials Science and Materials Engineering*; Elsevier, 2016.

(54) Hafner, A. Full Off-Specular and Specular Reflectometry for Soft Thin Film Analysis. Ph.D. Thesis, Université libre de Bruxelles, Faculté des Sciences—Physique: Bruxelles, 2019.

(55) de Gennes, P. G. Dynamics of fluctuations and spinodal decomposition in polymer blends. *J. Chem. Phys.* **1980**, *72*, 4756−4763.

(56) Sferrazza, M.; Heppenstall-Butler, M.; Cubitt, R.; Bucknall, D.; Webster, J.; Jones, R. A. L. Interfacial Instability Driven by Dispersive

Forces: The Early Stages of Spinodal Dewetting of a Thin Polymer Film on a Polymer Substrate. *Phys. Rev. Lett.* **1998**, *81*, 5173−5176.

(57) Good, R. J.; Girifalco, L. A. Theory for estimation of surface and interfacial energies. iii. estimation of surface energies of solids from contact angle data. *J. Phys. Chem. A.* **1960**, *64*, 561−565.

(58) Braslau, A.; Deutsch, M.; Pershan, P. S.; Weiss, A. H.; Als-Nielsen, J.; Bohr, J. Surface Roughness of Water Measured by X-Ray Reflectivity. *Phys. Rev. Lett.* **1985**, *54*, 114−117.

(59) Tylinski, M.; Chua, Y.; Beasley, M.; Schick, C.; Ediger, M. Vapor-deposited alcohol glasses reveal a wide range of kinetic stability. *J. Chem. Phys.* **2016**, *145*, No. 174506.

(60) Reiter, G.; Hamieh, M.; Damman, P.; Sclavons, S.; Gabriele, S.; Vilmin, T.; Raphaël, E. Residual stresses in thin polymer films cause rupture and dominate early stages of dewetting. *Nat. Mater.* **2005**, *4*, 754−758.

(61) Bäumchen, O.; Fetzer, R.; Jacobs, K. Reduced Interfacial Entanglement Density Affects the Boundary Conditions of Polymer Flow. *Phys. Rev. Lett.* **2009**, *103*, No. 247801.

(62) Debrégeas, G.; Martin, P.; Brochard-Wyart, F. Viscous bursting of suspended films. *Phys. Rev. Lett.* **1995**, *75*, 3886.

(63) Ashley, K. M.; Meredith, J. C.; Amis, E.; Raghavan, D.; Karim, A. Combinatorial investigation of dewetting: polystyrene thin films on gradient hydrophilic surfaces. *Polymer* **2003**, *44*, 769−772.

(64) Brochard-Wyart, F.; Debregeas, G.; Fondecave, R.; Martin, P. Dewetting of Supported Viscoelastic Polymer Films: Birth of Rims. *Macromolecules* **1997**, *30*, 1211−1213.

https://dx.doi.org/10.1021/acs.langmuir.0c02162
Langmuir 2020, 36, 12607−12619